Insights into directional scattering: from coupled dipoles to asymmetric dimer nanoantennas

AIMI ABASS,[1,*] **PHILIPP GUTSCHE,**[2] **BJORN MAES,**[3,4] **CARSTEN ROCKSTUHL,**[1,5] **AND EMILIANO R MARTINS**[6]

[1]*Institute of Nanotechnology, Karlsruhe Institute of Technology (KIT), P.O. Box 3640, 76021 Karlsruhe, Germany*
[2]*Zuse Institute Berlin, Takustr. 7, 14195 Berlin, Germany*
[3]*Micro- and Nanophotonic Materials Group, Faculty of Science, University of Mons, 20, place du Parc, B-7000 Mons, Belgium*
[4]*Photonics Research Group (INTEC), Ghent University-imec, Sint-Pietersnieuwstraat 41, B-9000 Ghent, Belgium*
[5]*Institute of Theoretical Solid State Physics, Karlsruhe Institute of Technology (KIT), Wolfgang-Gaede-Str. 1, 76131 Karlsruhe, Germany*
[6]*School of Engineering of São Carlos, University of São Paulo, Av. Trabalhador Saocarlense 400, São Carlos- SP, Brazil*
[*]aimi.abass@kit.edu

Abstract: Strong and directionally specific forward scattering from optical nanoantennas is of utmost importance for various applications in the broader context of photovoltaics and integrated light sources. Here, we outline a simple yet powerful design principle to perceive a nanoantenna that provides directional scattering into a higher index substrate based on the interference of multiple electric dipoles. A structural implementation of the electric dipole distribution is possible using plasmonic nanoparticles with a fairly simple geometry, i.e. two coupled rectangular nanoparticles, forming a dimer, on top of a substrate. The key to achieve directionality is to choose a sufficiently large size for the nanoparticles. This promotes the excitation of vertical electric dipole moments due to the bi-anisotropy of the nanoantenna. In turn, asymmetric scattering is obtained by ensuring the appropriate phase relation between the vertical electric dipole moments. The scattering strength and angular spread for an optimized nanoantenna can be shown to be broadband and robust against changes in the incidence angle. The scattering directionality is maintained even for an array configuration of the dimer. It only requires the preferred scattering direction of the isolated nanoantenna not to be prohibited by interference.

References and links

1. K. R. Catchpole and A. Polman, "Plasmonic solar cells," Opt. Express **16**(26), 21793–21800 (2008).
2. F. Priolo, T. Gregorkiewicz, M. Galli, and T. F. Krauss, "Silicon nanostructures for photonics and photovoltaics," Nat. Nanotechnol. **9**(1), 19–32 (2014).
3. N. X. A. Rivolta and B. Maes, "Angle-specific transparent conducting electrodes with metallic gratings," J. Appl. Phys. **116**(5), 053101 (2014).
4. Y. Fu and J. R. Lakowicz, "Modification of single molecule fluorescence near metallic nanostructures," Laser Photonics Rev. **3**(1-2), 221–232 (2009).
5. H. Aouani, O. Mahboub, N. Bonod, E. Devaux, E. Popov, H. Rigneault, T. W. Ebbesen, and J. Wenger, "Bright Unidirectional Fluorescence Emission of Molecules in a Nanoaperture with Plasmonic Corrugations," Nano Lett. **11**(2), 637–644 (2011).
6. J. Feng, T. Okamoto, and S. Kawata, "Highly directional emission via coupled surface-plasmon tunneling from electroluminescence in organic light-emitting devices," Appl. Phys. Lett. **87**(24), 241109 (2005).
7. S. Y. Zhang, G. A. Turnbull, and I. D. W. Samuel, "Enhancing the emission directionality of organic light-emitting diodes by using photonic microstructures," Appl. Phys. Lett. **103**(21), 213302 (2013).
8. S. Y. Zhang, G. A. Turnbull, and I. D. W. Samuel, "Highly Directional Emission and Beam Steering from Organic Light-Emitting Diodes with a Substrate Diffractive Optical Element," Adv. Opt. Mater. **2**(4), 343–347 (2014).
9. H. Elgala, R. Mesleh, and H. Haas, "Indoor Optical Wireless Communication: Potential and State-of-the-Art," IEEE Commun. Mag. **49**(9), 56–62 (2011).

10. A. Abass, S. R.-K. Rodriguez, T. Ako, T. Aubert, M. Verschuuren, D. Van Thourhout, J. Beeckman, Z. Hens, J. Gómez Rivas, and B. Maes, "Active Liquid Crystal Tuning of Metallic Nanoantenna Enhanced Light Emission from Colloidal Quantum Dots," Nano Lett. **14**(10), 5555–5560 (2014).
11. S. R. K. Rodriguez, S. Murai, M. A. Verschuuren, and J. G. Rivas, "Light-Emitting Waveguide-Plasmon Polaritons," Phys. Rev. Lett. **109**(16), 166803 (2012).
12. A. G. Curto, G. Volpe, T. H. Taminiau, M. P. Kreuzer, R. Quidant, and N. F. van Hulst, "Unidirectional Emission of a Quantum Dot Coupled to a Nanoantenna," Science **329**(5994), 930–933 (2010).
13. T. H. Taminiau, F. D. Stefani, F. B. Segerink, and N. F. Van Hulst, "Optical antennas direct single-molecule emission," Nat. Photonics **2**(4), 234–237 (2008).
14. A. Abass, S. R.-K. Rodriguez, J. Gómez Rivas, and B. Maes, "Tailoring Dispersion and Eigenfield Profiles of Plasmonic Surface Lattice Resonances," ACS Photonics **1**(1), 61–68 (2014).
15. J. Kim, Y. G. Roh, S. Cheon, U. J. Kim, S. W. Hwang, Y. Park, and C. W. Lee, "Directional radiation of Babinet-inverted optical nanoantenna integrated with plasmonic waveguide," Sci. Rep. **5**, 11832 (2015).
16. X. Ni, N. K. Emani, A. V. Kildishev, A. Boltasseva, and V. M. Shalaev, "Broadband light bending with plasmonic nanoantennas," Science **335**(6067), 427 (2012).
17. T. H. Taminiau, F. D. Stefani, and N. F. van Hulst, "Enhanced directional excitation and emission of single emitters by a nano-optical Yagi-Uda antenna," Opt. Express **16**(14), 10858–10866 (2008).
18. D. Dregely, R. Taubert, J. Dorfmüller, R. Vogelgesang, K. Kern, and H. Giessen, "3D optical Yagi-Uda nanoantenna array," Nat. Commun. **2**, 267 (2011).
19. J. Alda, J. M. Rico-Garcia, J. M. Lopez-Alonso, and G. Boreman, "Optical antennas for nano-photonic applications," Nanotechnology **16**(5), S230–S234 (2005).
20. L. Novotny and N. van Hulst, "Antennas for light," Nat. Photonics **5**(2), 83–90 (2011).
21. D. Vercruysse, Y. Sonnefraud, N. Verellen, F. B. Fuchs, G. Di Martino, L. Lagae, V. V. Moshchalkov, S. A. Maier, and P. Van Dorpe, "Unidirectional side scattering of light by a single-element nanoantenna," Nano Lett. **13**(8), 3843–3849 (2013).
22. T. Coenen, F. Bernal Arango, A. Femius Koenderink, and A. Polman, "Directional emission from a single plasmonic scatterer," Nat. Commun. **5**, 3250 (2014).
23. A. W. Powell, N. Hjerrild, A. A. R. Watt, H. E. Assender, and J. M. Smith, "Directional plasmonic scattering from metal nanoparticles in thin-film environments," Appl. Phys. Lett. **104**(8), 081110 (2014).
24. W. Yao, S. Liu, H. Liao, Z. Li, C. Sun, J. Chen, and Q. Gong, "Efficient Directional Excitation of Surface Plasmons by a Single-Element Nanoantenna," Nano Lett. **15**(5), 3115–3121 (2015).
25. T. Shegai, S. Chen, V. D. Miljković, G. Zengin, P. Johansson, and M. Käll, "A bimetallic nanoantenna for directional colour routing," Nat. Commun. **2**, 481 (2011).
26. A. Alù and N. Engheta, "Hertzian plasmonic nanodimer as an efficient optical nanoantenna," Phys. Rev. B **78**(19), 195111 (2008).
27. F. B. Arango, T. Coenen, and A. F. Koenderink, "Underpinning Hybridization Intuition for Complex Nanoantennas by Magnetoelectric Quadrupolar Polarizability Retrieval," ACS Photonics **1**(5), 444–453 (2014).
28. I. M. Hancu, A. G. Curto, M. Castro-López, M. Kuttge, and N. F. van Hulst, "Multipolar Interference for Directed Light Emission," Nano Lett. **14**(1), 166–171 (2014).
29. R. Alaee, R. Filter, D. Lehr, F. Lederer, and C. Rockstuhl, "A generalized Kerker condition for highly directive nanoantennas," Opt. Lett. **40**(11), 2645–2648 (2015).
30. I. Fernandez-Corbaton, "Forward and backward helicity scattering coefficients for systems with discrete rotational symmetry," Opt. Express **21**(24), 29885–29893 (2013).
31. I. Fernandez-Corbaton, M. Fruhnert, and C. Rockstuhl, "Dual and Chiral Objects for Optical Activity in General Scattering Directions," ACS Photonics **2**(3), 376–384 (2015).
32. J. Pomplun, S. Burger, L. Zschiedrich, and F. Schmidt, "Adaptive finite element method for simulation of optical nano structures," Phys. Status Solidi, B Basic Res. **244**(10), 3419–3434 (2007).
33. W. Lukosz, "Light-Emission by Magnetic and Electric Dipoles Close to a Plane Dielectric Interface. 3. Radiation-Patterns of Dipoles with Arbitrary Orientation," J. Opt. Soc. Am. **69**(11), 1495–1503 (1979).
34. W. Lukosz, "Theory of optical-environment-dependent spontaneous-emission rates for emitters in thin layers," Phys. Rev. B **22**(6), 3030–3038 (1980).
35. M. Albooyeh, R. Alaee, C. Rockstuhl, and C. Simovski, "Revisiting substrate-induced bianisotropy in metasurfaces," Phys. Rev. B **91**(19), 195304 (2015).
36. P. B. Johnson and R. W. Christy, "Optical Constants of the Noble Metals," Phys. Rev. B **6**(12), 4370–4379 (1972).
37. S. A. Maier, *Plasmonics: Fundamentals and Applications* (Springer, 2007).

1. Introduction

Directional scattering of light plays an important role in a wide range of photonic technologies such as photovoltaics [1–3], quantum emitters [4,5], light emitting diodes [6–8], and optical wireless communication [9]. These applications require meticulous control of the flow of light in order to be optimal. Through the usage of surface plasmon resonances in metallic nanoantennas, the benefits of having strong directional scattering and enhanced light-matter interaction can be combined to open up a plethora of functionalities [10–16]. One of the first strategies to achieve directional scattering from plasmonic nanoantennas has been the extrapolation of established designs from radiofrequency antennas to the visible. For example, it has been shown that the Yagi-Uda

antenna, which consists of multiple resonant elements with a spacing distance determined by phase matching conditions and suitably tuned resonance frequencies, can provide strong directivity in the optical domain [17–20]. The high directivity and efficiencies achieved from these earlier studies stimulated the quest for simpler and more compact geometries that can be fabricated more easily such as: single element nanoantennas [21–24], bimetallic structures [25], and plasmonic dimers [26]. Important insights have also been gained into the physics of directional scattering by nanoantennas and the role played by dipolar and multipolar sources [27–29].

It is of pertinence to note that symmetry properties have a significant impact on the scattering properties of nanoantennas [30,31]. Symmetric nanoantennas have intrinsic limitations with regard to providing a directionally specific response. One can expect to have the same scattering to angles of the same corresponding symmetry family. It is advantageous, therefore, to utilize asymmetric nanoantennas, which can potentially scatter light in an angularly more specific direction. Important examples of asymmetric structures investigated thus far include V shaped nanoantennas [21] and split ring resonators [28].

There remain, however, some challenges in light steering with single nanoantennas. Ensuring a narrow angular range of dominant scattering with a minimum number of elements in the nanoantenna structure has only been done with limited success. The local nature of a nanoantenna would naturally allow scattering into a continuum of directions. Therefore, decreasing the angular spread is likely to require additional complexity on the antenna geometry. Furthermore, the scattering response is typically sensitive to the angle of incidence and the wavelength of the illumination. Light steering by single nanoantennas thus still lacks the robustness that facilitates their applications in optoelectronic devices.

Here, we describe a simple design principle to achieve strong directional scattering into a higher index media based on the interference between two or more dipole sources' radiation. Once the requirement for achieving directionality is identified, we use these insights to demonstrate strong, directionally specific, fairly insensitive to angle of incidence, and broadband forward light scattering around the Total Internal Reflection (TIR) angle. All of these requirements are met by an easy to fabricate 2D asymmetric plasmonic dimer structure as sketched in Fig. 1 with geometries beyond the quasi-static regime.
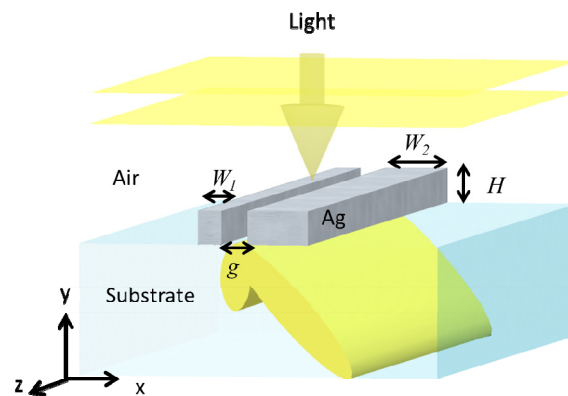

Fig. 1. Sketch of the asymmetric dimer nanoantenna.

The design of the asymmetric dimer nanoantenna is perceived by first considering the interference between multiple tangentially and normally oriented electric dipoles on top of a substrate. A strong and specific scattering into the TIR angle is obtained by tailoring the phase difference between the dipoles normally oriented to the substrate interface. The dipoles can be structurally implemented using fairly basic nanoantenna building blocks. Even though presented here for 2D systems, the design rationale can also be used to devise 3D structures. When the dimers are placed in an array configuration, the

preferential scattering direction is maintained as long as scattering to that particular direction is allowed.

Near- and far-field analyses are done using a finite element solver JCMsuite (JCMwave, Germany) [32]. As a proof of principle, we consider a nondispersive substrate (permittivity of 3.24) with a silver nanostructure and air on top. Only transverse magnetic (TM) polarized plane waves impinging from air are considered in the calculations.

2. Basic design principle

Our asymmetric dimer nanoantenna design was inferred by first considering the radiation pattern of electric dipolar line sources on top of the substrate. The associated current density is given by

$$\mathbf{J}(\mathbf{r},t) = A\delta(\mathbf{r} - \mathbf{r}_0)e^{-i\omega t}e^{i\phi}\mathbf{j} \tag{1}$$

Here, A is the real valued amplitude, ω is the angular frequency, $\mathbf{r}_0$ is the position of the line source with $|\mathbf{r}_0|^2 = x_0^2 + y_0^2$, $\mathbf{r}$ is the position in space, ϕ is the additional imparted phase, and $\mathbf{j}$ is a unit vector. Dipole line sources that are polarized horizontally to the substrate interface radiate predominantly in the forward direction [red dash plot in Fig. 2(a)] [33]. In contrast, dipole line sources that are oriented normal to the substrate can have an extremely narrow radiation pattern around the TIR angle of 33.75° in our case [blue line plot in Fig. 2(a)].
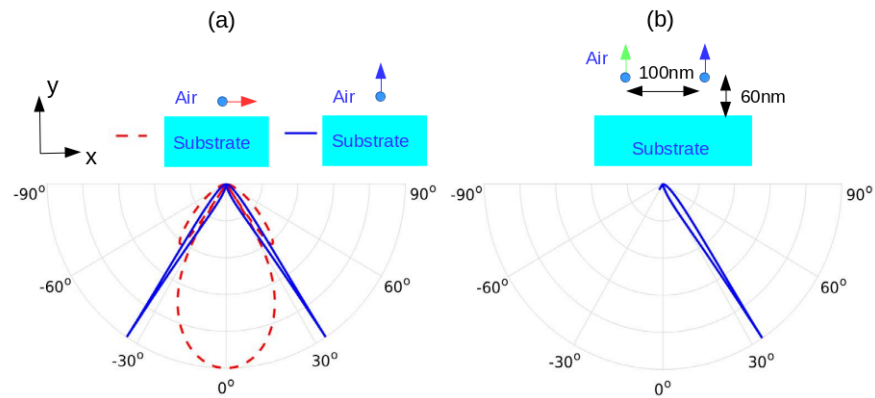

Fig. 2. (a) Far-field radiation patterns into the substrate of vertically and horizontally electric dipole line source placed 60nm above the substrate interface. The dashed red line corresponds to the radiation of the horizontally oriented electrical dipole and the blue solid line represents the radiation of the vertically oriented electrical dipole. (b) Radiation pattern of two vertically polarized dipole line sources with a phase difference of π/4 with respect to each other.

The radiation pattern of the dipole sources polarized normal to the substrate interface is mainly dominated by the dipole near-field (non-radiative) contribution that couples to the substrate and becomes radiative there [34]. The sharp and narrow radiation pattern reflects the fact that the dipole field component naturally peaks around the radiation edge in k-space. By changing the substrates' permittivity, the preferred radiation direction changes according to the TIR angle. When considering two dipole line sources that are both polarized normal to the substrate, their interference can produce a radiation pattern, which only goes to either the positive or negative TIR angle for a certain phase difference between the sources [Fig. 2(b)]. A nanoantenna design, which allows the excitation of such dipole moments with the corresponding phase difference, therefore results in a highly directional scattering into the substrate even if it is just a single nanoantenna. Furthermore, the exploitation of this dipole near-field coupling to substrate mechanism comes with the additional benefit of robustness against a change in the angle of incidence. As long as there is a net effective vertical dipole moment excited, and the distance of the

nanoantenna is close enough to the substrate to allow near-field coupling, there will always be a peak in the forward scattering around the TIR angle. We therefore aim to mainly harness these dipole moments that are normal to the substrate to produce our directional scattering.

Having identified the desired dipole moments, one can proceed to deduce the required geometry for certain plane wave incidence cases of interest. Here, we focus on achieving strong vertically polarized dipole moments around the normal incidence. Nanoantenna structures that support strong excitation of such dipole moments by normal incident plane waves naturally require a height for which the quasi-static approximation is no longer valid. No further restriction is needed. The substrate on top of which the nanoantennas are placed introduces a vertical asymmetry in the environment. This asymmetry, in turn, helps to induce higher order multipolar moments in the ridges, which contribute to the net effective vertical dipole moment. This effect is commonly known as substrate induced bi-anisotropy [35]. The nanoantenna height requirement can be relaxed, if the index contrast between the two dielectric media is made larger.

We proceed to show how we arrive at the geometry of Fig. 1. Ridge elements with a rectangular shape are chosen as the basic building blocks due to their simplicity. The width of the ridge is an additional parameter to control the wavelength at which optimum scattering will occur. A scan of the geometrical parameters is then performed to look for the geometry that would allow the excitation of vertical dipole moments by normal incident plane wave at the wavelengths of interest. One can expect that horizontal dipole moments are also being excited in the ridge structures. However, the contribution of the vertical dipole moment can still be dominant.

In Fig. 3(a) we show the polar plot of forward scattering into the substrate for an optimized single silver ridge for the wavelength of 530nm. The permittivity for silver is taken from Johnson and Christy [36]. By inspecting the scattered field profile, it can be seen that the ridge supports multipolar moments upon normal incident plane wave excitation. Despite this, the forward scattering into the substrate can be understood in terms of just three interfering electric line dipoles: one horizontally polarized dipole, and two anti-parallel vertically polarized dipoles placed at different positions [Fig. 3(a)]. For a single vertically polarized dipole, the portions of forward radiation into the substrate that go into the negative and positive angles have opposite phase. As the ridge structure has horizontal mirror symmetry, it necessarily supports two anti-parallel vertical dipole moments to produce a symmetric scattering pattern. The dipole parameter details we used to fit the numerical calculation can be found in Table 1 in the Appendix. Our dipole fitting reveals that the excited vertical electric dipole moments indeed give a dominant contribution to the ridge's forward scattering into the substrate. The contribution of the effective vertical electric dipole moments is the cause of the strong scattering around the TIR angle as seen in the forward scattering angular distribution in Fig. 3(a).

As already explained in the strategy, in order to direct the scattering around either the negative or positive TIR angle only, we need to modify the relative phase between the vertically oriented electric dipole moments. In our nanoantenna design, inducing the required phase difference was accomplished by adding a thinner ridge element to the side (Fig. 1). The purpose of the thinner ridge is to allow the excitation of a metal insulator metal (MIM) mode at the gap between the two plasmonic ridges [37]. While not affecting the forward scattering distribution on its own, the gap MIM mode affects the vertical charge oscillation around the gap region and in turn changes the relative phase of the effective vertical dipole moments. Thus, the usage of metal in our case is motivated by both the broadband response of localized plasmonic resonances and the possibility to excite gap MIM modes. The fact that the MIM mode can be excited at any incidence angle will contribute to the robustness of the asymmetric scattering pattern against change in angle of incidence. Guided by these design principles, optimization of the free geometrical parameters can be done to provide a strong, directional and asymmetric scattering response while being broadband and insensitive to angle of incidence.
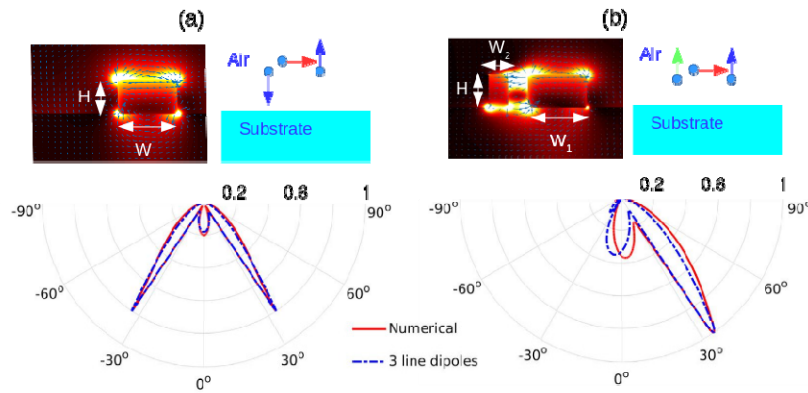
Fig. 3. Scattered far-field intensity into the substrate for (a) single ridge with H = 100nm and W = 150nm and (b) asymmetric dimer H = 100nm, W_1 = 50nm, and W_2 = 150nm in the case of normal incident light at the wavelength of 530nm. The scattered far-field intensity is compared to the radiation of multiple electric dipoles (2 vertically polarized and one horizontally polarized) with fitted parameters. The field profile plot shows the scattered field intensity while the arrows give the scattered field. All far-field plots are given in the same scale. Parameters used in the multiple electric dipoles model for both cases can be found in Table 1 and Table 2 respectively.

3. Most suitable structure

The near and scattering far-field plot for the optimized asymmetric ridge dimer around 530nm wavelength for normal incidence is shown in Fig. 3(b). The optimum parameters are: left ridge width W_1 = 50nm, right ridge width W_2 = 150nm, height H = 100nm, and gap width g = 50nm. In accordance with the design consideration, the thinner element with W_1 = 50nm is only weakly scattering at 530nm wavelength [Fig. 8(a)] and does not by itself affect the scattering characteristics to a notable extent. As seen in the inset of Fig. 3(b), the near-field profile of the asymmetric dimer reveals a more complex multipolar distribution than the case of a single ridge [inset of Fig. 3(a)]. The electromagnetic energy is mostly confined in the gap, which is partly due to a MIM mode being excited there [37]. A good fit of the numerically calculated scattering pattern can still be obtained with the three electric line dipoles model [Fig. 3(b), Table 2 in the Appendix] which is in agreement with the physical arguments described in the design rationale before. The optimized dimer scattering can actually be better represented with a four line dipoles model which considers an additional horizontally polarized dipole line source that is weaker in strength compared to the others (Fig. 9, Table 3 in the Appendix).

Throughout the 350-600nm wavelength range, an asymmetric forward scattering into the substrate is preserved with a peak around the positive critical angle of 33°. The polar plots of the far-field scattering into the substrate are shown in Fig. 4(a) for wavelengths of 400nm, 530 nm, and 600nm for a normal incident TM polarized plane wave. As a measure of the scattering strength and directivity, we define a forward scattering cross-section F, which is the ratio of the power scattered into the higher index substrate relative to the incoming plane wave intensity. For the wavelength of 530nm, 48.5% of the forward scattered power lies within the angular range of 30° - 60° with F = 346.7nm. The Full Width at Half Maximum (FWHM) of the lobe around the positive critical angle is 15°, which covers an even smaller portion of the angular range; indicating strong directivity. As a figure of merit to measure the scattering asymmetry, we define the parameter γ, which is the ratio of the scattered power portion going to the positive 30° - 60° range compared to the portion going to the negative range. γ amounts to 28.5 for a wavelength of 530nm at normal incidence. It indicates a strongly asymmetric scattering as the power scattered in the negative direction is 28.5 times less than in the positive direction. For the wavelength of 400nm, F = 211.4nm is obtained with 15.7% of the forward scattered power directed to the positive 30°- 60° angular range and with γ = 4.9. For a wavelength of 600nm, F = 313.4nm is obtained with 36.9% of the forward scattered power in the positive 30°- 60° angular range and with γ = 3.6 .
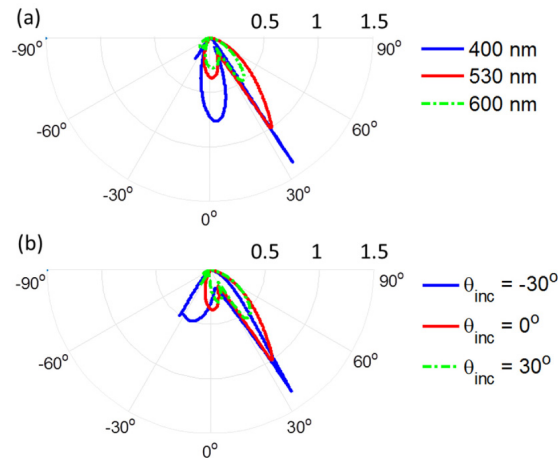
Fig. 4. (a) Scattered far-field intensity in the substrate at different incident wavelengths for the case of normal incident TM plane waves. (b) Scattered far-field intensity in the substrate at the wavelength of 530nm for different incoming angles θ_{inc}. All polar plots are shown for the optimized asymmetric dimer nanoantenna with $H = 100$nm, $W_1 = 50$nm, $g = 50$nm, and $W_2 = 150$nm. All the scattered far-field intensity plots are given in the same scale.

The preferential scattering to the positive critical angle direction at the wavelength of 530nm is maintained even up to ± 30° incidence angle [Fig. 4(b)]. For the case of + 30° angle of incidence, we obtain $F = 274.2$nm with 46.2% of the forward scattered power is in the positive angle and with $\gamma = 5.9$. For the case of −30° angle of incidence, $F = 410.6$nm is obtained with 34.1% of the forward scattered power in the positive direction and with $\gamma = 2.8$. For more oblique incidence (not shown here), the preferential scattering to the positive direction is no longer kept but there are still peaks around the critical angle.

One can actually obtain a more directionally specific nanoantenna system with less scattering around the normal direction with a thinner secondary ridge of 25nm width (Fig. 10). However, we found that the system is more sensitive to the incoming angle, particularly in the positive direction.

To demonstrate the broadband nature of the optimized asymmetric dimer scattering characteristics more clearly, a plot of the total scattering cross-sections, which includes both forward and backward scattering, is given in Fig. 5(a). It compares the scattering cross-section of the entire dimer (solid blue line) in Fig. 3(b) with that of the individual elements. The scattering cross-section spectra reveal multiple spectral features for all cases, which is an indication that each element supports multipolar resonances. Therefore, the geometry under consideration is beyond the quasi-static approximation at the wavelengths of interest. The dimer total scattering cross-section is dominated by the contribution of the larger ridge ($W_2 = 150$nm, dashed red line), which is also broadband in nature as it supports localized surface plasmonic (LSP) resonances. Notice that the scattering cross section of the dimer is higher than the scattering cross section of the single ridge. This higher scattering cross section is due to the excitation of the MIM mode, which contributes to a stronger horizontal dipole moment (compare Table 1 with Table 2 of the Appendix). The forward scattering angular distribution into the substrate at different wavelengths is shown in Fig. 5(b). It can be seen that the asymmetric scattering nature is most prominent in the wavelength region of 350 – 600nm. The sudden change in the scattering distribution around the TIR angle is maintained for all wavelengths.
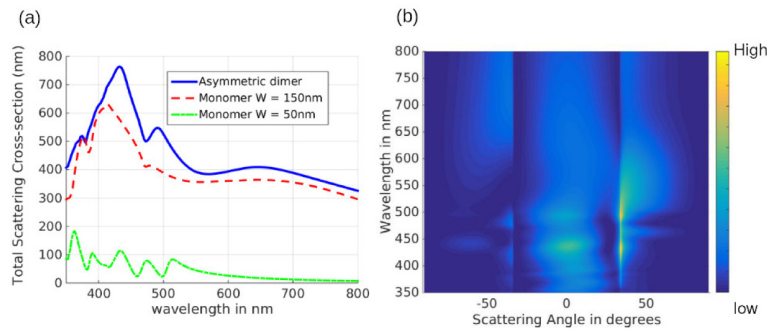
Fig. 5. (a) Total scattering cross-section spectra for the asymmetric dimer system compared to that of the single elements at normal incidence. All scattering cross-section spectra are normalized relative to the incoming plane wave intensity. (b) Angular distribution of the forward scattering into the substrate for different wavelengths at normal incidence.

The dimer configuration in Fig. 3(b) is not unique in providing asymmetric forward scattering patterns. One can essentially consider different width combinations between the dimer elements to tune the directionality of the antenna as shown in Fig. 6. Other dimer structures with both individual features supporting LSP resonances at the resonant wavelength can also have significantly asymmetric scattering around the TIR angle directions. If there are at least two vertical electric dipole moments being excited with the required phase difference and spatial displacement, one can attain a similar asymmetric scattering behaviour. In Fig. 6(a), where the left dimer is 50nm narrower than the right dimer, light is scattered mostly into the positive angles. In Fig. 6(b) the dimers have the same width and, as expected, the asymmetric scattering is lost due to the horizontal mirror symmetry of the structure. In Fig. 6(c), however, the left dimer is 50nm wider than the right dimer, and light is scattered mostly into the negative angles. Interestingly, the far-field of Fig. 6(a) is virtually the mirror image of the far-field of Fig. 6(c), which indicates that the phase difference between light scattered from the left and right ridges was reversed when the left ridge width went from 50nm shorter to 50nm larger than the right ridge. Utilizing larger ridge elements however, comes at the expense of a larger portion of power scattered around the normal direction. Interestingly, up to widths of 200nm, the entire dimer system can still be well fitted with only four electric dipole line sources (Fig. 11, Table 4 of the Appendix).

We thus see that only considering electric dipole moments can provide a congruent picture of the actual physics and provide design intuition even for such relatively large nanoantennas. One can also equivalently describe the nanoantenna scattering characteristics in terms of magnetic and electric multipolar moments. However, care needs to be taken since a non-optimal basis set may blur the physics and hinders easy design intuition.
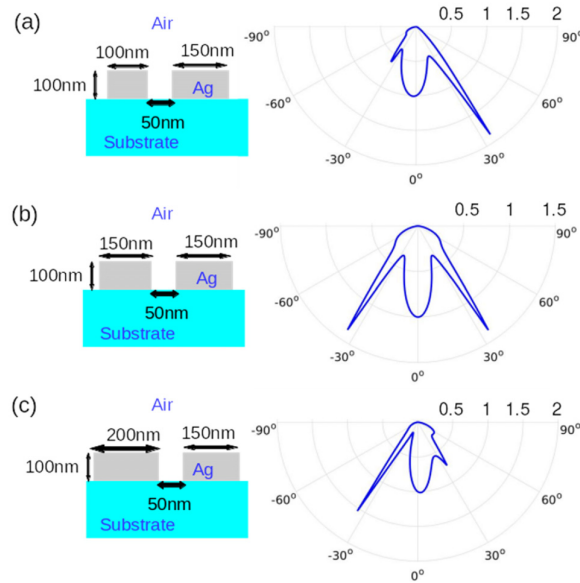
Fig. 6. Scattered far-field intensity into the substrate of several dimer nanoantennas with different width combinations for a normally incident TM polarized plane wave from air at a wavelength of 530nm.

4. Array configuration response

Finally, we use the asymmetric dimer of Fig. 3(b) as the unit cell of a grating and examine its diffraction properties. Figure 7(a) and 7(b) show the transmission for a respective grating with a period of 500nm as a function of the wavelength and the tangential wave vector component of the incident light $k_{\parallel,\text{inc}} = k_0 \sin(\theta_{\text{inc}})$ where k_0 is the vacuum wave vector and θ_{inc} is the angle of incidence from air. Normal incidence corresponds to $k_{\parallel,\text{inc}} = 0$. Figure 7(a) shows the transmittance towards the + 1 diffraction order which corresponds to diffraction to positive angle. Figure 7(b) shows the transmission for the −1 diffraction order. As is apparent from the figures, light is preferentially diffracted into the + 1 order for an extended spectral and angle of incidence range.

The striking difference between the diffraction efficiencies for the + 1 and −1 bands can be explained by the interplay between the diffracted light's parallel momentum and the scattering profile of the single dimer. This interplay is illustrated in Fig. 7(c), which shows the far-field intensity of the light scattered by the single dimer as a function of $k_{\parallel,\text{scat}}$ where $k_{\parallel,\text{scat}} = k_0 n_{\text{subs}} \sin(\theta_{\text{scat}})$ with θ_{scat} as the scattering angle under consideration and n_{subs} as the substrate index. Two illumination scenarios are considered. The blue/red solid line plots shows the far-field intensity distribution for light incidence with $k_{\parallel,\text{inc}} = +/- 0.0015$ rad/nm which corresponds to +/− 7.2° incidence angle. In both cases, the free space wavelength is 530nm. Notice that $k_{\parallel,\text{inc}}$ is the momentum of light propagating in air whereas $k_{\parallel,\text{scat}}$ [the x-axis of Fig. 7(c)] is the momentum of scattered light propagating in the substrate. The vertical dashed lines indicate the $k_{\parallel,\text{scat}}$ corresponding to the grating diffraction of orders + 1 and −1 for the respective incidence angles. Notice that the vertical dashed lines for the + 1 order lie on the edge of the high scattering lobe, which implies that for light incident with $k_{\parallel}$ between $k_{\parallel,\text{inc}} = -0.0015$ rad/nm and $k_{\parallel,\text{inc}} = 0.0015$ rad/nm, the single dimer optimal scattering angles coincide with the angles of constructive interference between adjacent dimers.
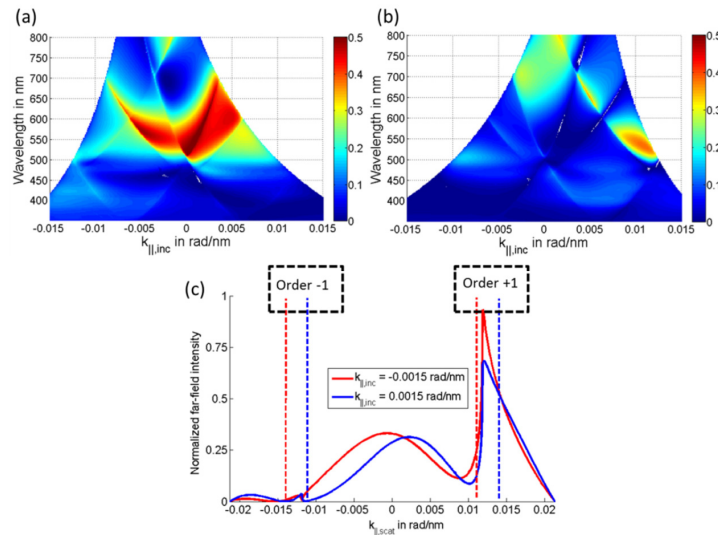
Fig. 7. Diffraction of a 500nm period grating which comprises of the single dimer of Fig. 3(b) as its unit-cell. (a) Transmittance towards the + 1 order. (b) Transmittance towards the −1 order. The grating exhibits strong (low) diffraction efficiency for the + 1 (−1) order over a large angle and wavelength range. (c) Scattering from one unit-cell as a function of the scattered light parallel momentum $k_{\parallel,scat}$ for two incidence conditions: incidence with $k_{\parallel,inc} = -0.0015$ rad/nm and incidence with $k_{\parallel,inc} = + 0.0015$ rad/nm. In both cases the free space wavelength is 530nm. Strong diffraction is achieved when the allowed by diffraction (vertical dashed lines) coincide with the $k_{\parallel,scat}$ exhibiting strong scattering from the unit-cell.

In other words, the unit-cell exhibits strong scattering into the + 1 order diffraction direction. This enhances the diffraction efficiency for this order [Fig. 7(a)]. The situation for the −1 order, on the other hand, is very different. As shown in Fig. 7(c), the vertical lines for the −1 order lie in the region of low scattering. The unit-cell does not scatter efficiently into the −1 order diffraction direction. This results in lower diffraction efficiencies [Fig. 7(b)]. Note that the period we examine here (500nm) is in the range of the spatial extension of a single dimer configuration which is 250nm. The closest gap between the elements of neighbouring unit cells is only 250nm. Even so, the directional preference of the individual unit cell can be carried over to the array configuration as long as the corresponding diffraction route is available.

5. Summary

In conclusion, we presented a simple design principle based on coupled dipolar sources to achieve strongly asymmetric directional scattering. We showed an asymmetric plasmonic dimer nanoantenna, which provides strong forward scattering cross sections with high directivity into a higher index medium around the TIR angle. The demonstrated robustness of the preferred scattering direction with respect to wavelength and incidence angle stems from the scattering mechanism reliance on the vertically oriented dipole moments' near-field coupling to the substrate. The utilization of LSP and MIM gap resonances further contributes to the broadband and angle insensitive performance of the directional scattering. The specific scattering directionality around the positive TIR angle was obtained by engineering the phase difference between the excited vertically oriented effective electric dipole moments. The scattering preference is maintained even when the dimers are set in an array configuration as long as the preferred direction of the single nanoantenna is not prohibited by interference. Even though relatively large geometries beyond the quasi-static limit were required, the design considers the radiation pattern of multiple electric dipole sources only, without the need to resort to higher order multipolar sources. Apart from the greater simplicity, we showed that the model provides a more intuitive and quite accurate physical picture of the coupling interaction in our ridge dimer

system, thus providing important insights into the physics of asymmetric directional scattering.

Appendix:

Tables 1-4 give the multiple dipole line sources calculation parameters to fit various nanoantenna structures discussed in the manuscript. The axes convention of the tables follows that indicated in Fig. 1. $y_0 = 0$nm corresponds to the interface of the substrate and positive values are on the air side. These parameters are input to Eq. (1) which describes the source terms used in the calculations.

Table 1 Single Ridge $W = 150$nm

	x_0 (nm)	y_0 (nm)	A (a.u)	ϕ (rad)	Polarization
Dipole 1	0	50	2	0	X
Dipole 2	−75	50	1	$−3\pi/4$	Y
Dipole 3	75	50	1	$\pi/4$	Y

Table 2 Dimer $W_1 = 50$nm $W_2 = 150$nm (3 dipoles)

	x_0 (nm)	y_0 (nm)	A (a.u)	ϕ (rad)	Polarization
Dipole 1	50	50	3.5	$\pi/10$	X
Dipole 2	25	50	1	$3\pi/4$	Y
Dipole 3	175	50	1	$11\pi/8$	Y

Table 3 Dimer $W_1 = 50$nm $W_2 = 150$nm (4 dipoles)

	x_0 (nm)	y_0 (nm)	A (a.u)	ϕ (rad)	Polarization
Dipole 1	100	50	1.8	0	X
Dipole 2	−25	50	0.5	0	X
Dipole 3	100	50	1	$3\pi/4$	Y
Dipole 4	−125	50	1	0	Y

Table 4 Dimer $W_1 = 200$nm $W_2 = 150$nm (4 dipoles)

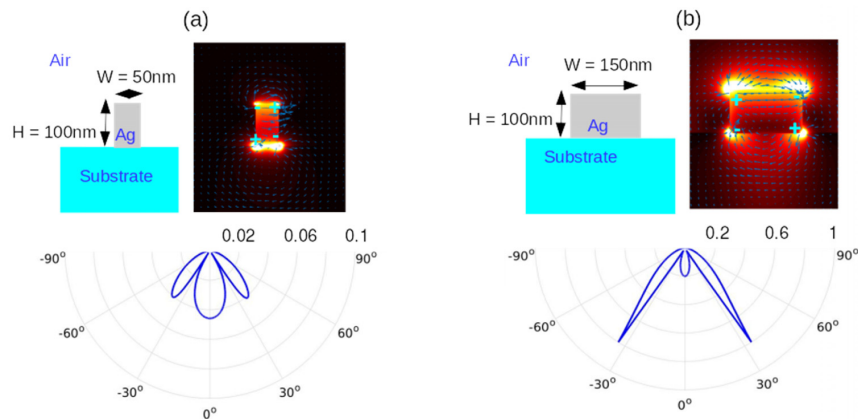|	x_0 (nm)	y_0 (nm)	A (a.u)	ϕ (rad)	Polarization
Dipole 1	100	50	1.7	$\pi/4$	x
Dipole 2	−125	50	1.7	$\pi/4$	x
Dipole 3	100	50	1	$\pi/2$	y
Dipole 4	−125	50	1	π	y

Fig. 8. Scattered near-field and substrate far-field of the individual ridges that comprise the dimer in Fig. 3(b). All ridges lie on top of the substrate and have height $H = 100$nm (a) ridge with width $W = 50$nm, (b) ridge width $W = 150$nm. The calculations were done for normal incidence at 530nm wavelength. Notice the difference of scale in the polar plots.
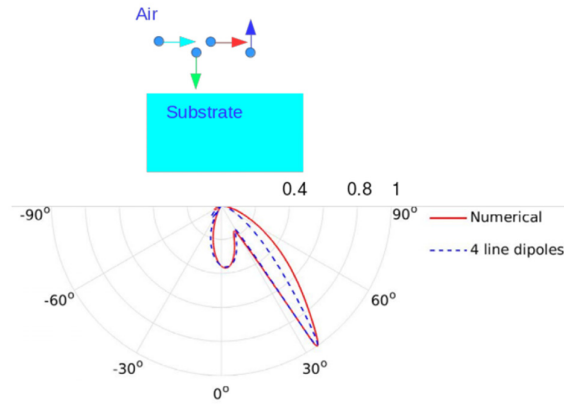
Fig. 9. Fit of the scattered far-field in the substrate for the case of Fig. 3(b) at 530nm wavelength with the radiation of four electric dipole line sources (2 horizontally polarized and 2 vertically polarized dipoles). The fitted parameters are given in Table 3.
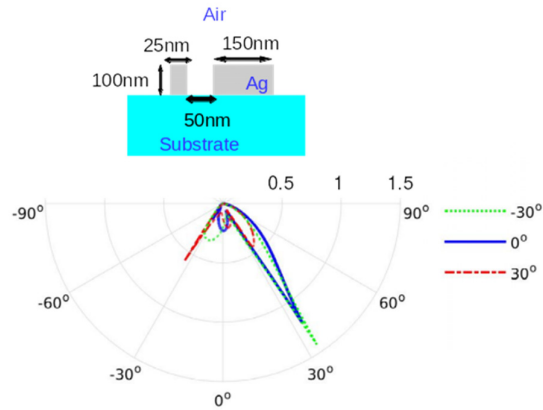

Fig. 10. Far-field angular distribution of the asymmetric dimer with the 50nm ridge replaced by a 25nm ridge. The employment of a thinner ridge enhances directionality at the expense of reduction in the tolerance against variations in the angle of incidence.
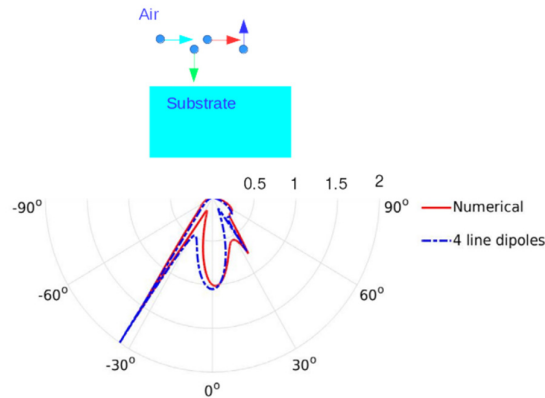

Fig. 11. Fit of the scattered far-field in the substrate for the case of Fig. 6(c) at 530nm wavelength to the radiation of four electric dipole line sources (2 horizontally polarized and 2 vertically polarized dipoles). The fitted parameters are given in Table 4.

Funding

Acknowledgment